Quaternary International 760 (2026) 110171

Contents lists available at ScienceDirect

Quaternary International

journal homepage: www.elsevier.com/locate/quaint

Geochemical changes of peat swamp sediments following fire in Southeastern Australia

Rebecca Ryan [a,*,1], Damien Lemarchand [b], Zoë Thomas [c,d], Ross Bradstock [e], Anthony Dosseto [a,e]

[a] Wollongong Isotope Geochronology Laboratory, School of Science, University of Wollongong, NSW, 2522, Australia
[b] Institut Terre et Environnement de Strasbourg, Université de Strasbourg-EOST, CNRS, ENGEES, 5 rue René Descartes, 67084, Strasbourg, Cedex, France
[c] Chronos 14 Carbon-Cycle Facility, Mark Wainwright Analytical Centre, University of New South Wales, NSW, 2052, Australia
[d] School of Geography and Environmental Science, University of Southampton, Southampton, SO17 1BJ, United Kingdom
[e] Centre for Environmental Risk Management of Bushfires, Institute for Conservation Biology and Management, University of Wollongong, Wollongong, NSW, 2522, Australia

ARTICLE INFO

Keywords:
Fire
Boron isotopes
Water quality
Southeastern Australia
Element concentrations

ABSTRACT

Retrospective measurements of fire characteristics, such as fire severity, can increase model data input and improve predictions of future fire events. However, existing records of past fire severity are limited to the recent past; therefore, there is a need to develop new proxies that can significantly extend our fire records. Boron isotopes and major element concentrations of the clay-sized fraction of sediments were used to assess fire severity and changes in water quality indicators as a result of fire, respectively, in three upland swamps in the Blue Mountains, southeastern Australia. The duration of the record varies across the three sites between 80 and 700 years as a result of varied sedimentation rates. Each site has a different fire history over the last 50 years, and the known fire record was used to corroborate fire signatures. Small increases in the Mg/Al and Ca/Al ratios were associated with fire-affected sediments, possibly due to increased wood ash input. However, the increased Ca/Al ratio was not preserved for older fire events. The P/Al and Fe/P ratios were shown to decrease with increasing depth, suggesting greater water saturation, whilst fire-affected sediments at two sites showed more oxic conditions, likely due to altered microbial activity. Mg and Al concentrations were shown to reflect the mineralogy of the basement, which is dominated by quartz with kaolinite and some calcite. The $\delta^{11}B$ value showed no significant correlation with known fires, possibly due to higher organic matter contributions to the clay-sized fraction overprinting the signature imparted to the clays from the fire. These results suggest that fires invoke changes in the concentration of major elements in sediments. However, further research is needed when applying the B isotope ratio to organic-rich sediments and for analysing changes in major element concentrations following older fire events.

1. Introduction

Fire has shaped terrestrial ecosystems across Australia for millennia (Sharples et al., 2016). Australia is the most fire-prone continent globally; however, fire regimes vary widely across the continent, controlled by vegetation structure, fuel loads and moisture content, and climate drivers (Bradstock et al., 2009). High inter-annual climate variability and extremes significantly alter fire dynamics and increase the potential for the development of 'mega fires' and 'fire storms' (Attiwill and Binkley, 2013; Sharples et al., 2016; Canadell et al., 2021). As climate change continues to alter the fire regime, it is expected that extreme fire weather and megafires will occur more frequently in the landscape; however, the magnitude of this change remains unknown (Keeley and Syphard, 2016). Retrospective measurements of fire characteristics, such as severity and intensity, can increase data input in model predictions of future fire events. Fire severity is defined as the proportion of above-ground biomass that is consumed, and ranges from low, where the fire is confined to the understorey, to extreme, where the canopy is completely consumed (Keeley, 2009; McLauchlan et al., 2020). Fire intensity is the rate of heat transfer and energy output from the fire front

* Corresponding author.
E-mail address: rjryan@caltech.edu (R. Ryan).
[1] Now at: The Isotoparium, Division of Geological and Planetary Sciences, California Institute of Technology, Pasadena, CA 91125, United States of America.

https://doi.org/10.1016/j.quaint.2026.110171
Received 3 September 2025; Received in revised form 11 November 2025; Accepted 12 February 2026
Available online 20 February 2026

(Byram, 1959).

Previous studies have used a variety of techniques to determine past fire characteristics from sediments, such as charcoal reflectance and pyrogenic carbon (PyC) (e.g. McParland et al., 2009; Belcher et al., 2018; Sawyer et al., 2018; Abney et al., 2019; Bird et al., 2019). Higher intensity fires, characterised by higher fire temperatures, have been shown to increase cell wall reflectance, suggesting its use as a proxy for fire intensity (McParland et al., 2009; Belcher et al., 2018). However, some bias may be introduced due to the brittle structure of charcoals formed at higher fire intensities, meaning these events may be overlooked in the record (McParland et al., 2009). Analysis of sediments by nuclear magnetic resonance (NMR) showed higher proportions of protein in sediments recording a high severity fire, compared with moderate severity fires (Abney et al., 2019). However, this differed from PyC, which showed a decrease in both protein and carbohydrates with increasing charring temperature (Abney et al., 2019). Remote sensing has also been used as a tool to assess the characteristics of active fires, fuel loading, fire spread and fire severity (Nedkov et al., 2018). These measures use such indices as Normalised Difference Vegetation Index (NDVI) and Normalised Burn Ratio (NBR) (Hammill and Bradstock, 2006; Malone et al., 2011; Gibson et al., 2020), however, the data is restricted to the satellite era (Mouillot and Field, 2005). Fire severity is important for determining ecosystem recovery post-fire; therefore, there is a need for new techniques to assess how fire severity has changed over the recent past.

Boron occurs in the natural environment almost exclusively bonded to oxygen, and has two stable isotopes, ^{10}B and ^{11}B (Vengosh et al., 1991; Hemming and Hanson, 1992). It is a key micronutrient for plants and performs a number of biogeochemical and physiological functions (Blevins and Lukaszewski, 1998; Cividini et al., 2010; Roux et al., 2015). Once used by plants, most B is used in the cell wall in an immobile form or is associated with sugar transport in a water-soluble form (Park and Schlesinger, 2002). Whilst a small amount of B is released to the atmosphere as plant aerosols, the majority of B is only returned to the soil surface during plant death (Park and Schlesinger, 2002). Boron is predominantly controlled by the vegetation cycle and experiences significant isotopic fractionation between different plant components, e.g. roots, leaves and bark (Gaillardet and Lemarchand, 2009; Cividini et al., 2010; Chetelat et al., 2021; Roux et al., 2022). Root uptake of soil solution occurs with minimal isotopic fractionation and is typically by passive diffusion, but it can also require active, high-affinity transport systems when the boron supply is low (Xu et al., 2015; Chetelat et al., 2021; Xiao et al., 2022). As the solution is transported from the roots to the leaves, it becomes isotopically heavier as the lighter isotope, ^{10}B, preferentially incorporates into the plant tissues (Geilert et al., 2015; Chetelat et al., 2021). Analysis of soils shows an enrichment in the heavier isotope following exposure to at least one high-severity fire (Lu et al., 2022). This was suggested to result from larger contributions of combusted leaves in ash, which was leached, allowing adsorption onto the surface of clays (Lu et al., 2022, 2024). Alluvial sediments recording a known high-severity fire have also shown an increase in the $\delta^{11}B$ value, suggesting the transportation of the fire signature to sediment deposits (Ryan et al., 2023). Ash formed from bark, however, has shown enrichment in the lighter isotope (Lu et al., 2022, 2024).

Fires are an important driver of the redistribution of elements and the associated impacts on peat sediment properties. The deposition of ash to surface peat following a fire event leads to an enrichment of cations such as calcium (Ca), magnesium (Mg), manganese (Mn), iron (Fe), sodium (Na) and zinc (Zn) (Dikici and Yilmaz, 2006; Könönen et al., 2015). Unlike carbon, these elements have higher volatilisation temperatures, so they accumulate even after very intense fires (Dikici and Yilmaz, 2006). Phosphorus (P) concentrations are more dependent on fire severity, with some studies suggesting an increase in P concentrations following low-to-moderate severity fires and a decrease following more intense fires (Dikici and Yilmaz, 2006; Sulwiński et al., 2020). Others suggest that high-temperature fires increase P concentrations in the upper soil layers, converting it to inorganic forms, thus increasing bioavailability for plants (D'Costa and Kershaw, 1995). Eucalypt litter ash has been found to contain varying amounts of Fe, Mn, Zn, copper (Cu), aluminium (Al), lead (Pb) and sulphur (S) (Khanna et al., 1994). Ash and fine sediment loads eroded post-fire can also increase stream turbidity, leading to more anoxic conditions and a heightened risk of eutrophication (Daniell and White, 2005). Whilst element composition has been used to assess the potential impacts of urbanisation on Temperate Highland Peat Swamps on Sandstone (THPSS) (Carroll et al., 2020), understanding post-fire changes in element composition remains largely unexplored. These upland swamps provide important refuges for fauna and hydrophilic flora post fire, and are important water sources for the Sydney Basin, particularly during periods of prolonged drought (Keith et al., 2023). Therefore, understanding any fire-induced changes to element composition post-fire is important for assessing any reductions in water quality or supply (Cowley et al., 2018).

This study applies B isotopes and major element concentrations to evaluate the severity of past fire events and the possible implications for water quality, respectively, in the Blue Mountains, a known fire-prone landscape in southeastern Australia. We aim to assess changes in fire severity and signatures of altered water quality over the recent past. It is expected that sediments recording fires that burnt at high severity show increases in the $\delta^{11}B$ value compared to sediments that do not record fire events. Aluminium (Al), calcium (Ca), magnesium (Mg), iron (Fe) and phosphorus (P) concentrations were also analysed and compared against the known fire record to determine changes through time and with exposure to fire. Loss on ignition (LOI) and X-ray Diffraction (XRD) were used to assess the changes in organic matter content and mineralogy of the sediments, respectively.

2. Methods

2.1. Study area

The Blue Mountains are approximately 60 km west of Sydney in New South Wales (NSW), Australia and form part of the Greater Blue Mountains World Heritage Area (Cunningham, 1984; Chapple et al., 2017). The underlying geology consists of sedimentary rocks, predominated by shales, coals and Triassic sandstones (Wilkinson et al., 2005; Aryal et al., 2018). The topography creates microclimates that control fire spread and affect fuel accumulation (Zhang et al., 2017). Dry sclerophyll forest covers much of the Blue Mountains and is highly flammable, and shows high rates of fuel accumulation (Collins et al., 2014). The canopy species typically resprout by epicormic buds and exhibit low rates of mortality at all fire intensities (Collins et al., 2014). Annual precipitation is 900–1000 mm, with sleet and occasional snow during winter and strong winds during warm summers (Wilkinson et al., 2005). Short-term decreases in precipitation and relative humidity can rapidly increase dry fuel connectivity, subsequently increasing the potential for large fire events (Caccamo et al., 2012; Nolan et al., 2016).

Temperate Highland Peat Swamps on Sandstone (THPSS) are present across the Blue Mountains and are a form of peatland occupying the headwaters of low-order streams (Fryirs et al., 2021). They are characterised by low slope and energy, and high rates of sediment accumulation and organic matter storage (Fryirs et al., 2021). THPSS support up to 4.6 million people and are listed as an endangered ecological community with important biodiversity and water quality significance (Fryirs et al., 2014b; Cowley and Fryirs, 2020). Anoxic conditions typically prevent decomposition, thus promoting water storage (Cowley et al., 2020). The water quality of the THPSS is naturally acidic, dilute, low salinity and sodium and chlorine ion-dominated, resulting in poor buffering capacity, making it highly susceptible to changes from external inputs, such as ash (Belmer et al., 2015; Carroll et al., 2019, 2020). THPSS are also vulnerable to extensive erosion due to disturbances, including anthropogenic, climate change and fire (Chalson and

Martin, 2009).

This study analyses sediments collected from three upland swamps in the Upper Blue Mountains: Corral Swamp (CS-01), Timmy's Swamp (TS-01) and Urella Brook Swamp (UBS-01) (Fig. 1). Each site has experienced a different recent fire history and fire return interval, and was selected to determine how fire severity has changed from 1957 to 2020 and assess the possible impacts these fire events may have had on water quality. Fire history was determined using remote sensing data and digitised fire line maps (Hammill et al., 2013; National Parks and Wildlife Service, unpublished data). These proxies were also compared against the fire events recorded using FTIR spectroscopy at these sites by Ryan et al. (2025).

2.2. Sample collection and age-depth model

In the field, sampling sites were selected such that they avoided creek lines and channels to ensure a more continuous record was collected. The surface of the swamps is largely treeless, dominated by heath vegetation, whilst the hillslope is dominated by dry sclerophyll forest. Hillslope soils are likely the predominant source of bushfire-derived sediment; thus, the distance from the treeline was also measured, ranging from 2 m (CS-01) to 8 m (TS-01). The three sites, CS-01, TS-01 and UBS-01 range in size from ~20 000 m^2 to ~43 000 m^2. An approximately 25 cm-deep monolith was collected to capture the recent past. The monolith was split in half vertically and subsampled at 1 cm intervals for isotopic and element concentration analysis. The radiocarbon-based age-depth model is based on Ryan et al. (2024, 2025) (UBS-01) (Supplementary Table 1 and Supplementary Fig. 1).

2.3. X-ray Diffraction (XRD)

X-ray Diffraction (XRD) analysis was used to determine the mineralogy of swamp sediments. Bulk samples from the top, middle and bottom of the Corral Swamp (CS-01) and Long Swamp (LS-02) sites were analysed by XRD at the University of Wollongong. Given the similarity between sites and samples from different depths, as well as the predominance of Hawkesbury Sandstone across the entire Sydney Basin, it is expected that the TS-01 and UBS-01 sites would have comparable mineralogy to CS-01 and LS-02. Due to the high organic matter content of the bulk samples, a combination of hydrogen peroxide and heating was used to remove organic material. The samples were mounted in aluminium holders and placed in a Thermo Fisher ARL Equinox 1000 diffractometer. They were loaded and analysed through an automatic sample holder for 90 min with an incidence angle of 6 and a beam

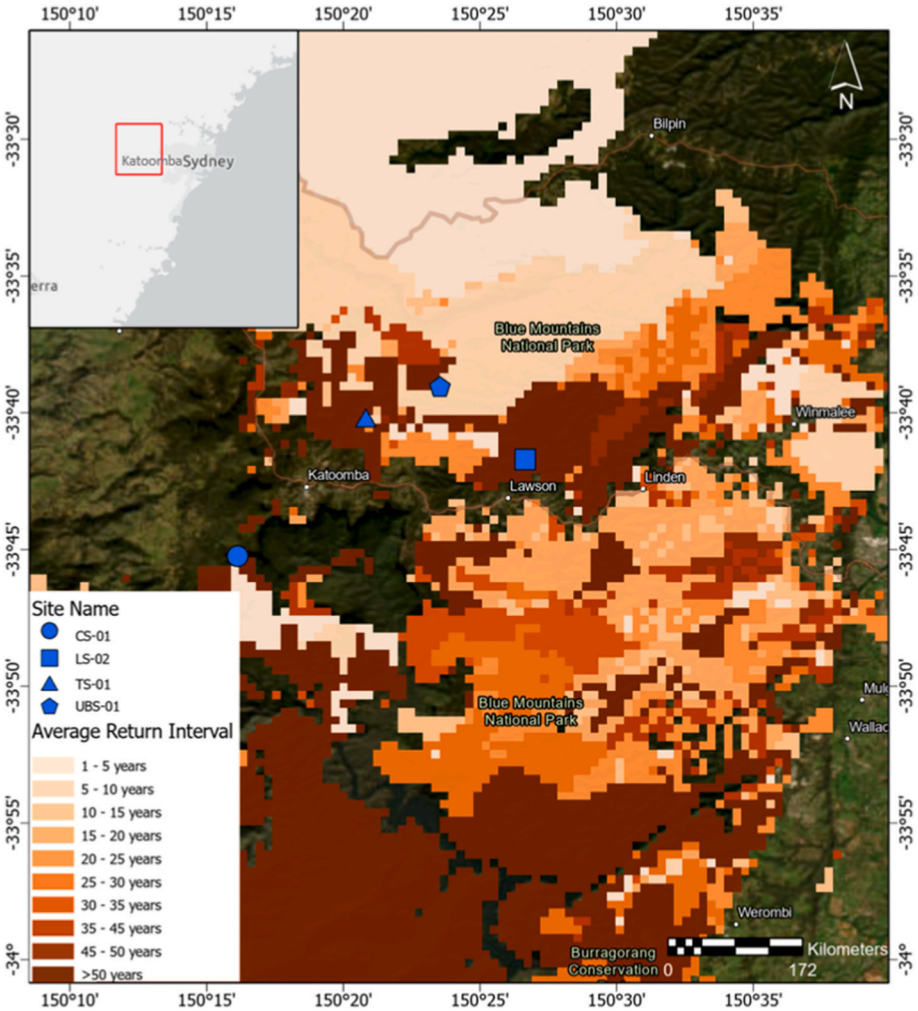

Fig. 1. Average fire return interval map for the Blue Mountains, New South Wales, Australia, taken from Ryan et al. (2025), showing the sites studied as a) Corral Swamp (CS-01, blue circle), b) Long Swamp (LS-02, blue square, only analysed for XRD), c) Timmy's Swamp (TS-01, blue triangle) and d) Urella Brook Swamp (UBS-01, blue pentagon). Unshaded areas have not been burnt during the period from 1957–2020. Data adapted from NPWS unpublished data and © State Government of NSW and Department of Planning and Environment 2010, Satellite Image: Esri, Maxar, GeoEye, Earthstar Geographics, CNES/Airbus DS, USDA, USGS, AeroGRID, IGN and the GIS User Community Esri, HERE, Garmin, © OpenStreetMap contributors and the GIS User Community. (For interpretation of the references to colour in this figure legend, the reader is referred to the Web version of this article.)

geometry of 2.5 mm × 0.1 mm with copper x-ray tubing. Operating potential and current were 35 kV and 28.8 mA, respectively. Samples were analysed between 4 and 70° 2θ at 2° per minute with a step size of 0.02. The spectra produced were analysed in the Match! software to determine the mineral phases present in each sample.

2.4. Loss on ignition (LOI)

Loss on ignition was used to determine the organic matter content of the clay fraction from each of the three sites (CS-01, TS-01 and UBS-01). Clay samples were heated in a muffle furnace at 550 °C for 8–9 h. Organic contributions to the clay fraction were determined using the mass difference before and after heating.

2.5. Boron isotopes and content

The clay-sized fraction of sediments from the three monoliths, CS-01, TS-01 and UBS-01, were prepared and analysed for B isotopes at the Wollongong Isotope Geochronology Laboratory (WIGL). LS-02 was not analysed for B isotopes or major element concentrations due to lack of clay availability. Approximately 50 mg of each sub-sample was combined with potassium carbonate in a 1:5 flux for alkali fusion at 950 °C. The resulting solid was dissolved in HCl and 18.2 M-Ω water by sonication, and the supernatant was isolated by centrifugation for chromatography. A two-step ion chromatography method was employed to isolate B for isotopic analysis (Lemarchand et al., 2012). First, 5 mL of solution was loaded onto a column containing 1.5 mL of BIORAD AG50W-X8 resin for cation exchange chromatography. Boron is not retained on the resin, and the elution was collected. Boron was further eluted with 2 mL of 0.01 M HCl. The resulting solution was then pH-adjusted to 8–10 using 0.5 M NaOH that was previously purified using a column loaded with Amberlite IRA 743 resin. Each sample was then loaded onto a column containing 0.5 mL of Amberlite IRA 743 resin. The matrix was eluted in water. Sodium chloride (0.5 M) was then loaded to replace anions with chlorine, and an additional matrix elution with water removed sodium. Boron was then eluted in 0.5 M HCl. Due to the high organic matter content of the samples, an additional sublimation step was required to improve the homogeneity of the final elution by separating boron from the dissolved organic matter, prior to analysis (Gaillardet et al., 2001). A 0.5 mL aliquot of the final elution solution was pipetted into the lid of a PFA vial. The vial was then closed upside down to ensure the 0.5 mL droplet remained in the lid. The lid was then tightly wrapped in aluminium foil and placed on its lid on a hotplate at 110 °C for 3 h, following Roux et al. (2015). The samples were then allowed to cool for 20 min before slowly rotating the solution to capture the condensation from the walls of the vial. This was repeated for 4 aliquots for each sample to ensure adequate B concentrations for analysis by multi-collector inductively coupled plasma mass spectrometry (MC-ICP-MS).

Boron isotopes were measured by MC-ICP-MS with a Thermo Fisher Neptune Plus™ at WIGL. The sample introduction system consisted of a standard sample and H skimmer cone, a PFA nebuliser with a flow rate of approximately 100 μL min^{-1} and a Scott Cyclonic Spray Chamber. ^{10}B and ^{11}B were collected in Faraday cups coupled with a 10^{11}-Ω resistor. Tuning was performed to gain a sensitivity of 0.5 V of ^{11}B per 50 ppb of B in the primary standard, NIST SRM 951a. Measurements were performed in low-resolution mode. Standard-sample-standard bracketing was used to correct for mass bias. ERM AE120 was analysed as a secondary standard at the beginning and end of each analysis sequence. The total procedure blank was 8.3 ± 2.4 ng B (2SE; n = 11). Mean measured $\delta^{11}B$ values for ERM AE120 was −20.53 ± 0.25‰ (2SE; n = 18), which is within error of the expected value (−20.2 ± 0.6‰; Vogl and Rosner, 2012). Mean measured $\delta^{11}B$ values for USGS W2-a reference material was 11.77 ± 0.53‰ (2SE; n = 12) which is within error of the recommended value (12.2 ± 0.4‰; Gangjian et al. 2013). Precision was assessed by analysing replicate samples (n = 3), giving a 2SE of ±0.30‰.

Boron concentration was also measured using MC-ICP-MS with a Thermo Fisher Neptune Plus™ at WIGL. The intensity on ^{11}B of each sample solution was compared to that of the 50 ppb primary standard. B concentration was then determined using the masses of the sample solution analysed by MC-ICP-MS, the solution loaded onto the cationic exchange column and the mass of the clay sample processed by alkali fusion.

2.6. Major element composition

The clay size fraction after removal of organic matter was analysed for major element concentrations. Approximately 30 mg of each sample and USGS BHVO-2 reference material were dissolved in HF and HNO_3, followed by aqua regia and H_2O_2. The samples were redissolved in 0.3 M HNO_3 and then diluted 1:10. Major element concentrations were measured using a Perkin Elmer Optima 8000 inductively coupled plasma optical emission spectrometer (ICP-OES) at WIGL. The sample introduction system consisted of a concentric glass nebuliser and quartz spray chamber. Concentrations of each element were calibrated using 100 ppm multi-element standards (PerkinElmer TruQ), diluted to 0.5, 1, 5, 10, 25 and 50 ppm, ensuring that the r-squared value of the calibration curve was >0.995 for each element. Measured values for the BHVO-2 Hawaiian Volcano Observatory Basalt were within error of the certified value for Mg, Fe and Al and just outside of the expected range for Ca and P (Table 1). Two replicates were analysed to assess precision, showing 2SE values of ±0.39% (Al), ±0.02% (Ca), ±0.25% (Fe), ±0.01% (Mg) and ±0.02% (P).

3. Results

3.1. X-ray Diffraction (XRD)

The results show a predominance of quartz in all of the samples, averaging ~70 % or greater for all except for one sample analysed (Supplementary Fig. 2). Kaolinite is also present, ranging from 16 to 70% abundance. Three samples across the two sites showed the presence of calcite (4–18%).

3.2. Loss on ignition (LOI)

The organic matter content ranges from 26 to 60 wt%, 22 to 78 wt% and 23 to 73 wt% for CS-01, TS-01 and UBS-01, respectively. In TS-01, LOI decreases with increasing depth; however, there is no systematic trend with depth in CS-01 or UBS-01 samples (Supplementary Fig. 3).

3.3. Radiocarbon age-depth model

The age-depth models were determined by Ryan et al. (2025) using OxCal 4.4 (Bronk Ramsey, 2009) and produced sedimentation rates in line with those previously observed in the Blue Mountains (Fryirs et al., 2014a; Freidman and Fryirs, 2015). Due to large differences in sedimentation rate, the three sites record different durations of time and therefore, have different resolutions, recording ~80 years, ~200 years and ~700 years for TS-01, CS-01 and UBS-01, respectively.

Table 1
Certified and measured values for USGS BHVO-2 Basalt reference material.

Element	Certified Value	Measured Value (2SD; n = 2)
Magnesium	4.38 ± 0.03%[a]	4.55 ± 0.33%
Calcium	8.15 ± 0.04%[a]	8.39 ± 0.03%
Phosphorus	0.12 ± 0.01%[a]	0.07 ± 0.03%
Iron	8.67 ± 0.07%[a]	8.78 ± 0.62%
Aluminium	7.11 ± 0.03%[a]	7.09 ± 1.21%

[a] Determined from certified values of oxides.

3.4. Boron isotopes

The boron (B) isotope composition ranges from −0.58 to 4.45‰, −8.19 to 2.51‰ and −3.47 to 1.75‰ for CS-01, TS-01 and UBS-01, respectively. The CS-01 site shows positive excursions in the $\delta^{11}B$ value at 11–13 cm and 14–15 cm (Supplementary Fig. 4A), corresponding to deposition years of 1917 (+44/–85)–1907 (+47/–94) CE and 1887 (+66/–160) CE, respectively (Fig. 2A). A significant negative excursion is evident at 9–10 cm, corresponding to 1938 (+36/–68) CE. The TS-01 site shows a small positive excursion in the $\delta^{11}B$ value at 4–5 cm, corresponding with 2000 (+16/–7) CE and negative excursions at 12–13 cm and 14–15 cm, corresponding to 1979 (+11/–7) CE and 1974 (+9/–8) CE, respectively (Fig. 2B). Finally, the UBS-01 site shows peaks in the $\delta^{11}B$ value at 3–4 cm, 6–7 cm, and 11–12 cm (Supplementary Fig. 4C), corresponding with deposition years of 1987 (+17/–59) CE, 1935 (+50/–81) CE and 1848 (+106/–117) CE (Fig. 2C). A negative excursion can be seen at 19–20 cm depth, which corresponds with deposition years of 1661 (+186/–110) CE. There appears to be no clear relationship between the B isotope composition of the clay-sized fraction of sediments and fire-affected sediments at any of the three sites. There is also no significant correlation between the B isotope ratio and any of the element concentrations measured.

Boron content in the clay-sized fraction of sediments averages ~15 ppm at the three sites. Peaks are seen in the CS-01 site at 10–11 cm and 16–17 cm, corresponding to deposition years of 1928 (+39/–77) CE and 1877 (+73/–166) CE, respectively (Supplementary Fig. 5A and D). The TS-01 site shows positive excursions at 2–3 cm, 12–13 cm and 15–16 cm, corresponding with years of 2006 (+17/–8) CE, 1979 (+11/–7) CE and 1971 (+9/–7) CE (Supplementary Fig. 5B and E). The peaks at 12–13 cm and 15–16 cm depth correspond with negative excursions in the $\delta^{11}B$ value. There is no obvious trend with increasing depth. Finally, the UBS-01 site shows relatively constant B contents from 12 to 23 cm corresponding to the period from 1576 (+219/–103)–1830 (+117/–123) CE (Supplementary Fig. 5C and F). Above this, there is then a gradual decrease in B concentration with decreasing depth until the top 3 cm of the monolith, where B content once again increases from 3 to 0 cm. There is no correlation between changes in the B isotope ratio and B content at any of the three sites.

3.5. Major element concentrations

Aluminium concentrations at CS-01 range from 6.4 to 38.7 wt%. Two samples at CS-01 show significantly higher Al concentrations than the remaining samples ($p = 0.039$), with concentrations of 38.7 wt% (7–8 cm) and 33.9 wt% (9–10 cm), corresponding with deposition years of 1959 (+28/–51) CE and 1938 (+36/–68) CE (Fig. 3A). Below 8 cm depth, a general increasing trend with depth is observed (Fig. 3). The Al concentration of the TS-01 site ranges from 6.5 to 15.8 wt%, and negative excursions are observed at 7–8 cm and 19–20 cm, corresponding with deposition years of 1992 (+14/–7) CE and 1960 ± 7 CE, respectively (Fig. 3B), the latter of which corresponds with a fire-affected layer from the aromatic/aliphatic ratio in Ryan et al. (2025). The Al content at the UBS-01 site ranges from 9.1 to 19.9 wt% with a generally increasing trend with depth (Fig. 3C). The sediments at 0–2 cm, corresponding to a deposition period of 2011 (+3/–31)–2017 (+2/–10) CE, were identified as fire-affected layers. Like TS-01, there appears to be a decrease in Al content at 1–2 cm. Aluminium was used to normalise the concentrations of the other major elements studied, as it is largely unaffected by biological processes and is a conservative element that is not impacted by anthropogenic processes (Liaghati et al., 2003; Rönspieß et al., 2020). Extractable Al is typically associated with finer particles; therefore, it has been commonly used for normalisation to correct for the grain size effect (Liaghati et al., 2003).

The Ca content is low across all sites, averaging 0.066 wt% with a general decreasing trend with increasing depth. It ranges from 0.029 to 0.091 wt% at CS-01, 0.011 to 0.11 wt% at TS-01 and 0.020 to 0.39 wt% at UBS-01 (Supplementary Fig. 7A–C). The Ca/Al ratio shows the same general trend with depth as the Ca concentration alone and shows

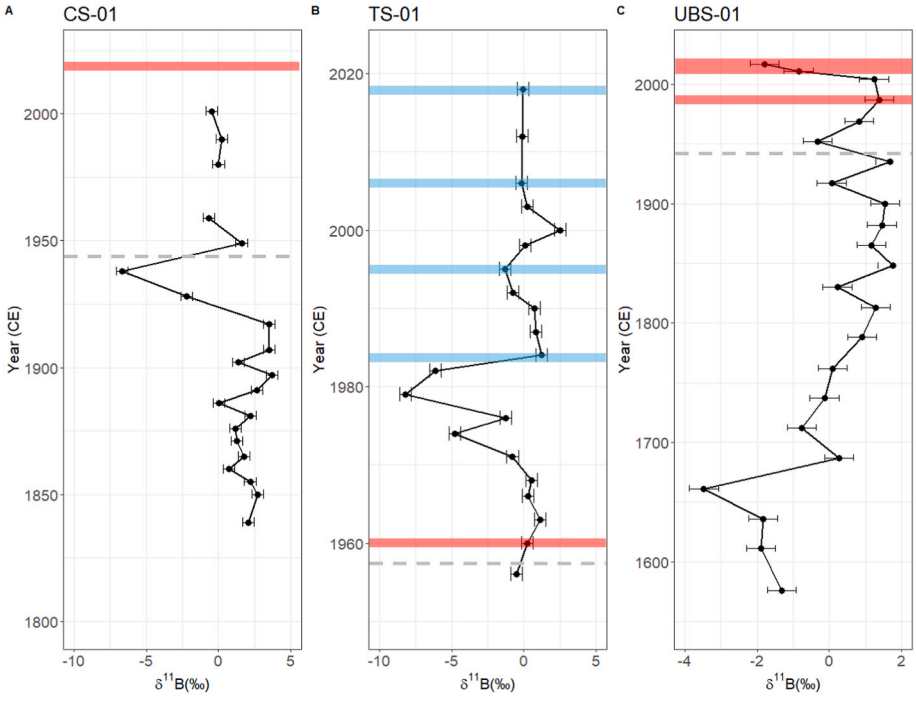

Fig. 2. $\delta^{11}B$ value (in ‰) as a function of modelled deposition year (in CE) for A) Corral Swamp (CS-01), B) Timmy's Swamp (TS-01) and C) Urella Brook Swamp (UBS-01). Gaps in the CS-01 profile are due to lack of clay availability for analysis. Shaded bars represent fires from the known fire record between 1957 and 2020, where red shading represents fires identified in Ryan et al. (2025) using the aromatic/aliphatic ratio of FTIR spectra in sediments, and blue shading represents fires in the known record that were not correlated with peaks in the aromatic/aliphatic ratio. The grey dotted line represents the extent of the known fire record. *(For interpretation of the references to colour in this figure legend, the reader is referred to the Web version of this article.)*

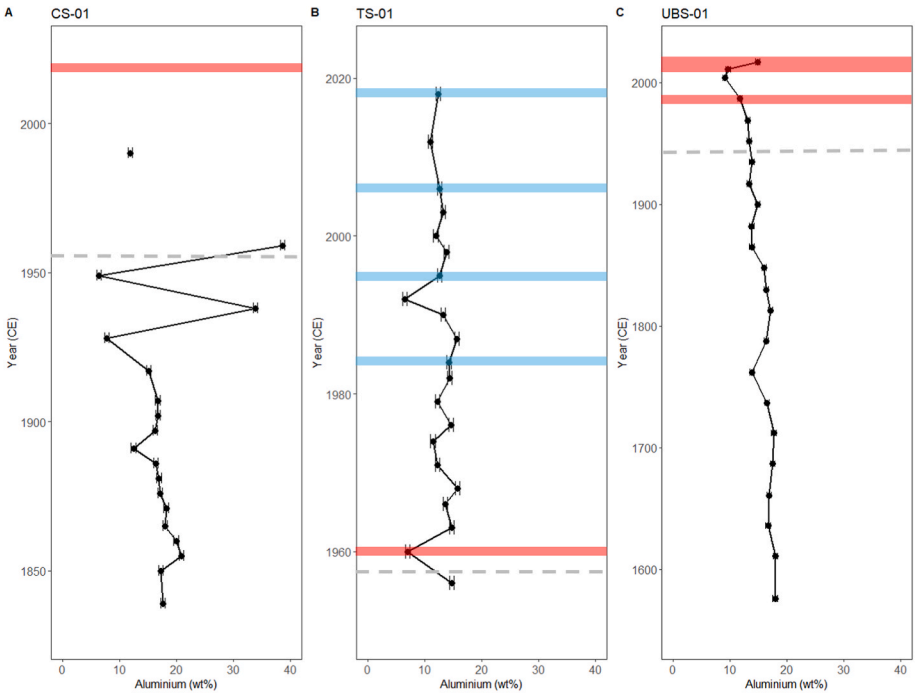

Fig. 3. Aluminium concentration (in wt%) as a function of modelled sediment deposition year (in CE) for A) Corral Swamp (CS-01), B) Timmy's Swamp (TS-01) and C) Urella Brook Swamp (UBS-01). Gaps in the CS-01 profile are due to lack of clay availability for analysis. Shaded bars represent fires from the known fire record between 1957 and 2020, where red shading represents fires identified in Ryan et al. (2025) using the aromatic/aliphatic ratio of FTIR spectra in sediments, and blue shading represents fires in the known record that were not correlated with peaks in the aromatic/aliphatic ratio. The grey dotted line represents the extent of the known fire record. (For interpretation of the references to colour in this figure legend, the reader is referred to the Web version of this article.)

smaller variation at the CS-01 site compared with TS-01 and UBS-01. It ranges from 0.29 to 0.84, 0.085 to 0.91 and 0.11 to 4.04 at the CS-01, TS-01 and UBS-01 sites, respectively (Fig. 4).

The average Mg content across the 3 sites is 0.23 wt%. The concentration is low across all sites, ranging from 0.08 to 0.5 wt% at CS-01, 0.1 to 0.3 wt% at TS-01, and 0.2 to 0.4 wt% at UBS-01 (Supplementary

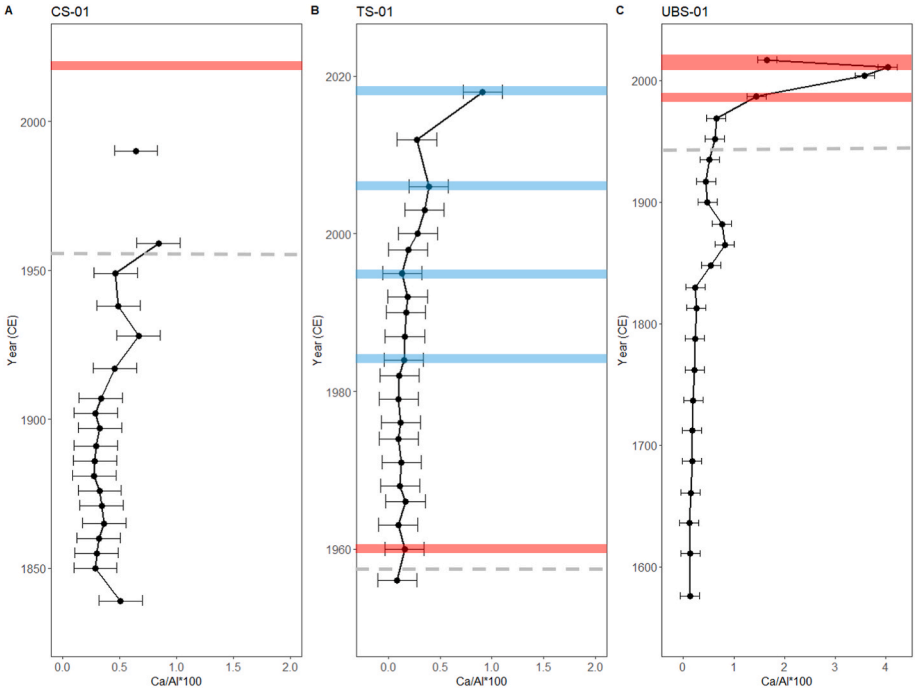

Fig. 4. Ca/Al ratio (unitless) as a function of modelled sediment deposition year (in CE) for A) Corral Swamp (CS-01), B) Timmy's Swamp (TS-01) and C) Urella Brook Swamp (UBS-01). Gaps in the CS-01 profile are due to lack of clay availability for analysis. Shaded bars represent fires from the known fire record between 1957 and 2020, where red shading represents fires identified in Ryan et al. (2025) using the aromatic/aliphatic ratio of FTIR spectra in sediments, and blue shading represents fires in the known record that were not correlated with peaks in the aromatic/aliphatic ratio. The grey dotted line represents the extent of the known fire record. (For interpretation of the references to colour in this figure legend, the reader is referred to the Web version of this article.)

Fig. 8). The Mg concentration was normalised to Al. Mg/Al ratios range from 0.83 to 1.5, 1.5 to 3.5, and 1.1 to 4.1 for CS-01, TS-01, and UBS-01, respectively. The Mg/Al ratio displays a general decreasing trend with increasing depth across all sites, with some correlation with the aromatic/aliphatic ratio for the fire events at 1–2 cm in the UBS-01 monolith and 19–20 cm in the TS-01 profile, corresponding with deposition years of 2011 (+3/–31) and 1960 ± 7 CE, respectively (Fig. 5). There is no significant correlation with fire events in the CS-01 site.

The P content averages 0.88 wt% across the three sites, where concentrations are higher in the CS-01 site, compared with TS-01 and UBS-01. It ranges from 0.51 to 3.8 wt% at CS-01, 0.2 to 0.8 wt% at TS-01, and 0.21 to 1.1 wt% at UBS-01 and shows a general decreasing trend with increasing depth below 5 cm at the UBS-01 site (Supplementary Fig. 9). The concentration remains comparable across all depths at the TS-01 site, with the exception of peaks at 0–1 cm, 9–10 cm and 15–16 cm, corresponding with deposition years of 2018 (+3/–2) CE, 1987 (+13/–7) CE and 1971 (+9/–7) CE, respectively. Phosphorus concentrations at CS-01 show a general increasing trend with increasing depth from ~10 cm. The P concentration was normalised to Al. At the CS-01 site, the P/Al ratio ranged from 6.2 (13–14 cm) to 12.4 (4–5 cm) and shows no consistent trend with depth (Fig. 6A). At TS-01, the P/Al ratio ranges from 2.1 (16–17 cm) to 6.2 (0–1 cm) and showed a general decreasing trend with increasing depth. Peaks are observed at 0–1 cm, 9–10 cm, 15–16 cm and 19–20 cm depth, corresponding with deposition years of 2018 (+3/–2) CE, 1987 (+13/–7) CE, 1971 (+9/–7) CE and 1960 ± 7 CE, respectively (Fig. 6B). Finally, the UBS-01 site shows P/Al ratios ranging from 1.3 (20–21 cm) to 8.8 (4–5 cm). Similar to the TS-01 site, P concentrations at UBS-01 show a general decreasing trend with increasing depth. Two peaks are observed at 2–3 cm and 4–5 cm depth, corresponding with deposition years of 2004 (+6/–51) CE and 1969 (+28/–65) CE (Fig. 6C).

Iron concentration ranges from 2.4 to 19.6 wt%, 0.8 to 2.9 wt% and 3.0 to 9.6 wt% at CS-01, TS-01 and UBS-01, respectively (Supplementary Fig. 10). Fe concentrations at the TS-01 and UBS-01 sites show a general decreasing trend with increasing depth. However, there is no clear trend in the CS-01 site. When normalised to Al, the Fe/Al ratio ranges from 0.1 to 0.6, 0.1 to 0.2 and 0.2 to 0.7 at the CS-01, TS-01 and UBS-01 sites, respectively (Fig. 7). The Fe/Al ratio at all three sites shows a general decreasing trend with increasing depth. The CS-01 site also shows a peak at 13–18 cm depth, corresponding with a deposition year range of 1872 (+76/–164) CE to 1892 (+63/–172) CE.

The Fe/P ratio ranges from 1.3 to 8.9, 1.8 to 5.0 and 5.6 to 15.4 for CS-01, TS-01 and UBS-01, respectively (Fig. 8). The CS-01 and UBS-01 sites show an increased Fe/P ratio for fire-affected layers identified from the aromatic/aliphatic ratio at 1887 (+66/–170) CE (CS-01) and 0–1 cm (UBS-01). However, there is a peak at 20–21 cm depth in the UBS-01 site that is not associated with a fire event identified by the aromatic/aliphatic ratio in the FTIR spectra. At the TS-01 site, however, the Fe/P ratio shows a decrease in the fire-affected layer at 1960 ± 7 CE.

4. Discussion

4.1. Boron isotopes

The boron isotope ratio of the clay-sized fraction was hypothesised to inform on fire severity. Using the expected depths of sediments recording fire events determined in Ryan et al. (2025), there is no clear relationship between the $\delta^{11}B$ value and fire events in any of the three sites (Fig. 2). Ryan et al. (2025) analysed bulk sediments from all three sites using FTIR spectroscopy, showing that the aromatic/aliphatic ratio increased for sediments recording known high-intensity fire events. However, some of the known fire events have not been recorded in the FTIR spectrum of the sediments. This was hypothesised to be the result of insufficient rainfall post-fire to mobilise sediments (Ryan et al., 2025). In the Australian context, high-intensity fire events are typically canopy-consuming (Bradstock et al., 2010; Collins et al., 2014); therefore, it was expected that sediments with high aromatic/aliphatic ratios

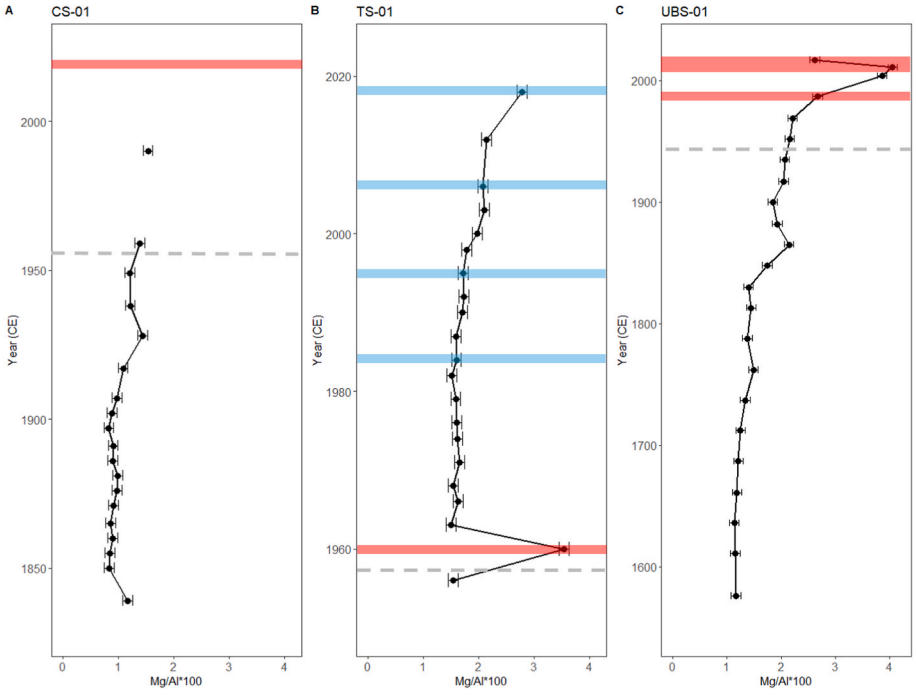

Fig. 5. Mg/Al ratio (unitless) as a function of modelled sediment deposition year (in CE) for A) Corral Swamp (CS-01), B) Timmy's Swamp (TS-01) and C) Urella Brook Swamp (UBS-01). Gaps in the CS-01 profile are due to lack of clay availability for analysis. Shaded bars represent fires from the known fire record between 1957 and 2020, where red shading represents fires identified in Ryan et al. (2025) using the aromatic/aliphatic ratio of FTIR spectra in sediments, and blue shading represents fires in the known record that were not correlated with peaks in the aromatic/aliphatic ratio. The grey dotted line represents the extent of the known fire record. (For interpretation of the references to colour in this figure legend, the reader is referred to the Web version of this article.)

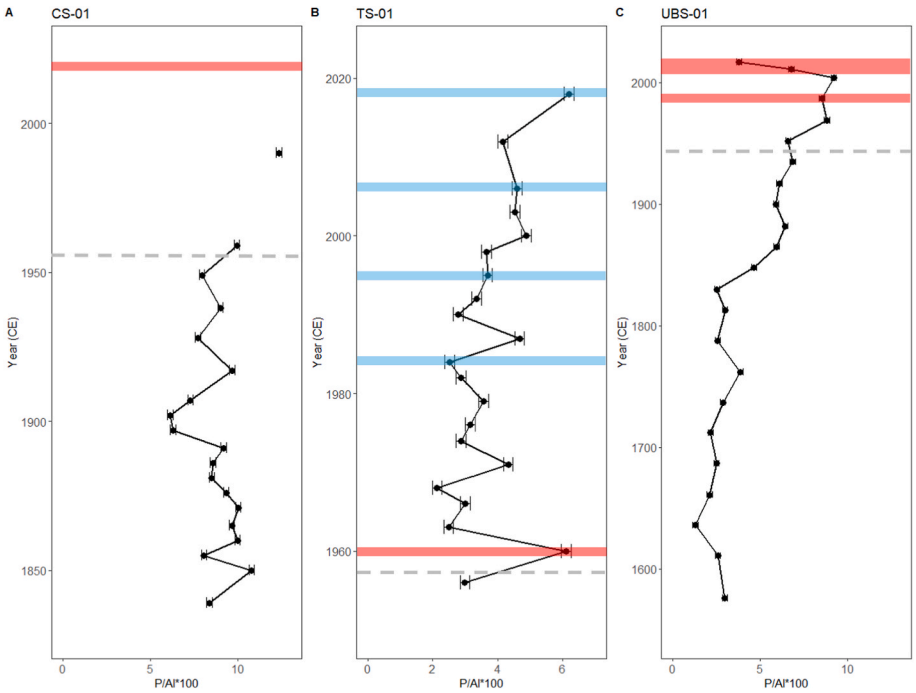

Fig. 6. P/Al ratio (unitless) as a function of modelled sediment deposition year (in CE) for A) Corral Swamp (CS-01), B) Timmy's Swamp (TS-01) and C) Urella Brook Swamp (UBS-01). Gaps in the CS-01 profile are due to lack of clay availability for analysis. Shaded bars represent fires from the known fire record between 1957 and 2020, where red shading represents fires identified in Ryan et al. (2025) using the aromatic/aliphatic ratio of FTIR spectra in sediments, and blue shading represents fires in the known record that were not correlated with peaks in the aromatic/aliphatic ratio. The grey dotted line represents the extent of the known fire record. (For interpretation of the references to colour in this figure legend, the reader is referred to the Web version of this article.)

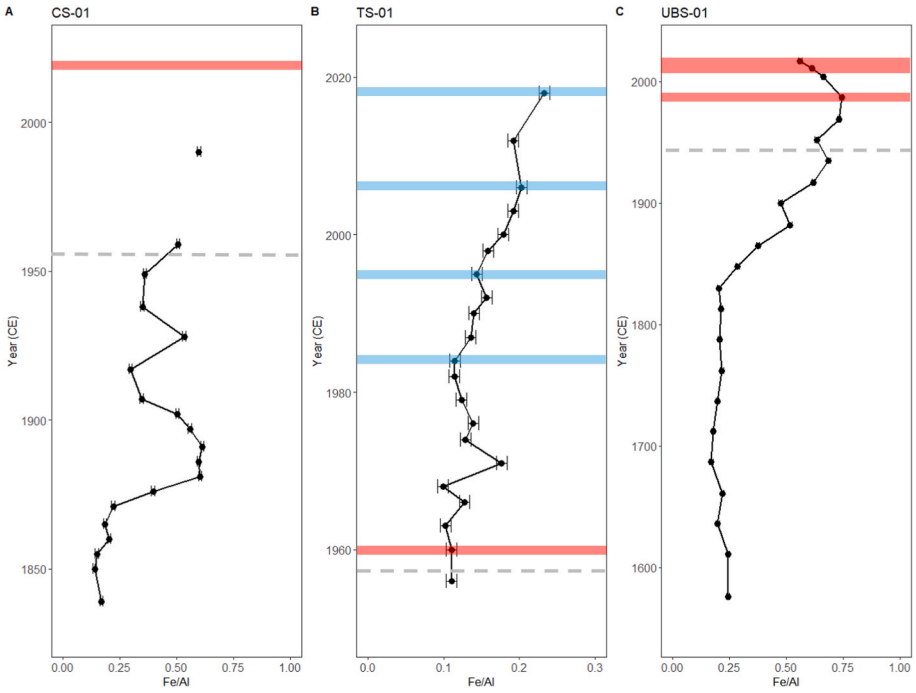

Fig. 7. Fe/Al ratio (unitless) as a function of modelled sediment deposition year (in CE) for A) Corral Swamp (CS-01), B) Timmy's Swamp (TS-01) and C) Urella Brook Swamp (UBS-01). Gaps in the CS-01 profile are due to lack of clay availability for analysis. Shaded bars represent fires from the known fire record between 1957 and 2020, where red shading represents fires identified in Ryan et al. (2025) using the aromatic/aliphatic ratio of FTIR spectra in sediments, and blue shading represents fires in the known record that were not correlated with peaks in the aromatic/aliphatic ratio. The grey dotted line represents the extent of the known fire record. (For interpretation of the references to colour in this figure legend, the reader is referred to the Web version of this article.)

would also show increased $\delta^{11}B$ values.

The three sites have a high organic matter content, particularly in the clay-sized fraction, as illustrated by LOI values in clay fractions of up to 80%. LOI is a measure of the organic matter content lost by heating at 550 °C and is a proxy for organic matter content. Soil organic matter content influences boron adsorption onto clays. More boron is typically

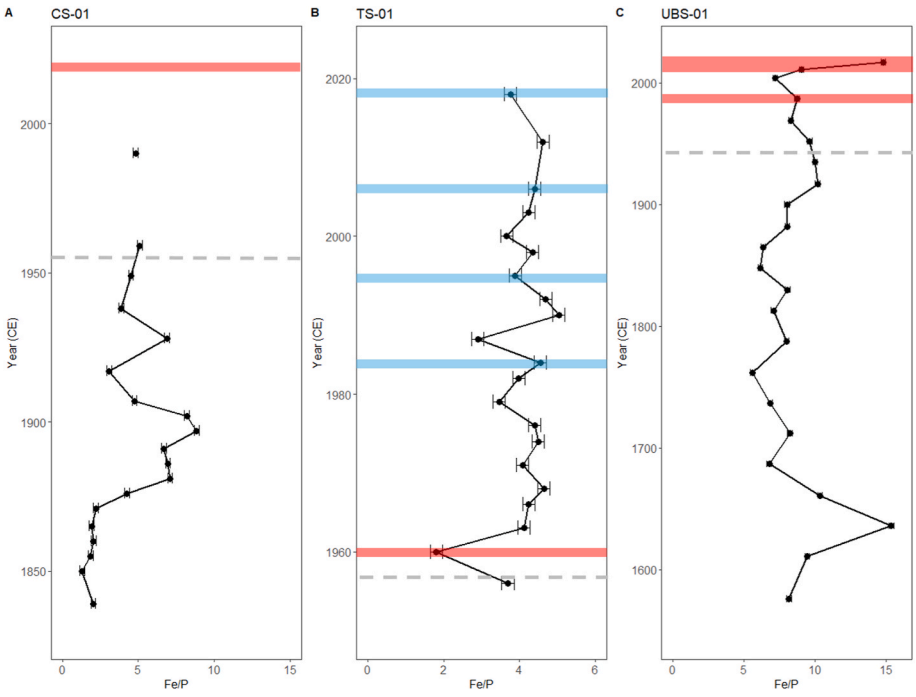

Fig. 8. Fe/P ratio (unitless) as a function of modelled sediment deposition year (in CE) for A) Corral Swamp (CS-01), B) Timmy's Swamp (TS-01) and C) Urella Brook Swamp (UBS-01). Gaps in the CS-01 profile are due to lack of clay availability for analysis. Shaded bars represent fires from the known fire record between 1957 and 2020, where red shading represents fires identified in Ryan et al. (2025) using the aromatic/aliphatic ratio of FTIR spectra in sediments, and blue shading represents fires in the known record that were not correlated with peaks in the aromatic/aliphatic ratio. The grey dotted line represents the extent of the known fire record. (For interpretation of the references to colour in this figure legend, the reader is referred to the Web version of this article.)

adsorbed onto soil organic matter than onto inorganic mineral soils, due to competitive adsorption (Yermiyahu et al., 2001; Goldberg and Suarez, 2012; Goli et al., 2019). Kaolinite, which is the dominant clay mineral in the THPSS sediments, contains ~7 ppm of B (Fleet, 1965). This is compared to the up to several 100's ppm of B present in organic matter (Goodarzi and Swaine, 1994; Williams et al., 2001). Therefore, it is most likely that the changes in $\delta^{11}B$ are a reflection of the B isotope composition of the organic matter, which is overprinting any changes to the clay fraction post-fire. The positive excursions resulting from fire events observed by Ryan et al. (2023) occurs over a relatively narrow range compared to existing studies of plant material, which can range from ~−9 to +24 ‰ (Roux et al., 2022). Therefore, the fire signature imparted to the clay-sized fraction of the three swamps may be overprinted by the organic matter contributions to the <2 μm fraction.

Lu et al. (under review) analysed the $\delta^{11}B$ values of leachates from charcoals formed at different fire severities. The natural variation of $\delta^{11}B$ values between individual trees did not overprint changes invoked by combustion, assuming lithology was comparable. Leachates from bark combusted at low severity showed higher $\delta^{11}B$ values compared to leachates from moderate to extreme severity fires. This was hypothesised to result from the possible crossing of a temperature threshold during fires of moderate severity or above that increases volatilisation of ^{11}B, thus enriching ^{10}B in the charcoal fraction. Therefore, in organic-rich sediments, where the B isotope signature imparted to the clay-sized fraction from the fire may be overprinted by the organic fraction, analysis of the B isotope composition of the charcoal fraction may be more suitable for distinguishing fire severity.

4.2. Major element concentrations

High concentrations of Al were expected in the swamp samples due to the predominance of kaolinite. Aluminium associated with clays is important because it influences the physical properties of clays and their reactions with organic and inorganic anions (Smith and Emerson, 1976). Decreases in Al content were associated with fire-affected sediments identified in the known fire record and may result from dilution caused by increased deposition of other ions in the form of ash (Könönen et al., 2015).

The Ca/Al ratio has been used to determine the presence of $CaCO_3$ in sediments (Sundararajan and Natesan, 2010). Combustion of wood mineralises a number of elements, resulting in the formation of carbonates and hydroxides, which are enriched in Ca, among other alkaline metals (Etiegni and Campbell, 1991). Calcium carbonate is typically formed at temperatures between 350 and 400 °C and increases rapidly with fire intensity; however, this is dependent on the plant species burnt (Quintana et al., 2007). Ash deposition can significantly alter the pH range of the swamps, disrupting natural ionic balance and nutrient distribution as well as increasing natural weathering rates. Therefore, it is important to understand how this has changed through time. The Ca content was normalised to Al to determine possible changes in $CaCO_3$ content attributed to wood ash inputs. The peaks in the aromatic/aliphatic ratio at 1882 (+84/–101) CE and 1737 (+157/–121) CE in the UBS-01 site, 1960 ± 7 in the TS-01 site, and 1887 (+66/–160) CE in the CS-01 site are not associated with increases in the Ca/Al ratio. The hydrological regime of upland swamps is complex and varies widely between individual swamps. The THPSS are largely groundwater driven, where increased water levels typically peak 1–2 days after the rainfall event (Hardwick, 2020). This is due to the porous, fibric soils of the top ~50 cm, which efficiently absorb and redistribute rainwater (Fryirs et al., 2014a). In undisturbed swamps, a strong nutrient gradient exists, where slope and elevation can create different environmental and drainage conditions, and vegetation distributions (Keith and Myerscough, 1993). Ca is highly labile and susceptible to leaching (Lampela et al., 2014). Therefore, it is possible that contributions from ash were redistributed in short succession following the fire, and concentrations were not high enough to induce any long-term changes to the pH or overall swamp system.

A peak in the Ca/Al ratio is evident at the surface of the TS-01 and

UBS-01 sites and may correspond to the 2019–20 "Black Summer Bushfires". In the case of the TS-01 site, there was no peak in the aromatic/aliphatic ratio corresponding to the 2019–20 bushfires. This may suggest that there was some burning of the heath vegetation, resulting in an increase in the Ca/Al ratio; however, this is unlikely given that grass fuels typically produce much lower quantities of ash (Cook, 1994). Previous studies have shown increased Ca content in the surface sediments of swamps as a result of vegetation redistribution (Weiss et al., 2002). Thus, this may explain the increased Ca/Al ratio at the surface of the TS-01 and UBS-01 monoliths.

Mg concentrations can also reflect the contributions from wood ash (Demeyer et al., 2001). Magnesium requires temperatures greater than 1107 °C for volatilisation (Dikici and Yilmaz, 2006). Studies from a fire event in southwest Victoria found that 16–40 wt% of Mg was lost to the smoke column (Flinn et al., 1979), therefore, the majority of Mg concentrates in the wood ash fraction during a fire event, even after a high-severity fire (Dikici and Yilmaz, 2006; Pereira et al., 2012). Higher Mg/Al ratios are associated with peaks in the aromatic/aliphatic ratio of sediments recording fire events in 2011 (+3/–31) CE (UBS-01) and 1960 ± 7 CE (TS-01), suggesting greater correlation with the fire-affected sediments than the Ca/Al ratio. However, there is also a peak in the Mg/Al ratio at the surface of the TS-01 site. Francos et al. (2020) found that the increase in the Ca/Al ratio were typically confined to short periods after the fire event. This may explain the correlation with the Mg/Al ratio at the surface of the swamp, while the sediments recording older fire events are not associated with a peak in the Ca/Al ratio.

The Mg/Al ratio can also be used as an indicator for the composition of clay minerals that are transported to a catchment (Sundararajan and Srinivasalu, 2010; Natalicchio et al., 2019). Low Mg/Al ratios typically reflect the predominance of Mg-poor clay minerals, whilst higher Mg/Al ratios are indicative of more Mg-enriched minerals such as chlorite (Sundararajan and Srinivasalu, 2010; Natalicchio et al., 2019). As shown by the XRD data, the mineral fraction of the swamp sediments is dominated by quartz and kaolinite, both of which are Mg-depleted (Mayland and Wilkinson, 1989). Therefore, the low Mg/Al ratios likely indicate the predominance of Mg-depleted minerals throughout the recorded period.

A strong positive correlation is seen between the P/Al and Fe/Al ratios at both TS-01 and UBS-01 sites, with correlation coefficients of 0.91 and 0.65, respectively. This is in agreement with previous studies, which also show a strong correlation between P/Al and Fe/Al ratios (Hinrichs et al., 2001; Rönspieß et al., 2020). The CS-01 site shows a correlation coefficient of −0.18. This may be due to missing data due to insufficient clay content for analysis, resulting in fewer data over a small range. Iron and Al oxides have a high sorption capacity for organic and inorganic-bound P, particularly when they are in amorphous forms (Niedermeier and Robinson, 2009; Kjaergaard et al., 2012). Low P/Al and Fe/Al ratios have been associated with anoxic conditions (Hinrichs et al., 2001; Sundararajan and Natesan, 2010; Sundararajan and Srinivasalu, 2010). When conditions are anoxic, Fe(III) oxides are subjected to microbial-induced reductive dissolution, which results in the release of adsorbed phosphate into solution (Kjaergaard et al., 2012). The P/Al and Fe/Al ratios of both TS-01 and UBS-01 show a general decreasing trend with increasing depth. This could suggest increasingly anoxic conditions with increasing depth, possibly resulting from increased water saturation or microbial activity with depth (Kjaergaard et al., 2012). Fire layers identified from the FTIR spectra in all three sites also show higher P/Al and Fe/Al ratios, suggesting more oxic conditions. Fire-affected sediments typically experience reduced microbial activity due to modifications to microbial communities (Certini, 2005; Guénon et al., 2013), suggesting a greater retention of P in these layers.

The Fe/P ratio has been used to assess whether sediments are absorbing or desorbing P into the pore water (Sulwiński et al., 2020). Lower Fe/P ratios have been suggested to indicate that soluble P is unable to be retained by the sediments and is released into the water fraction (Norgbey et al., 2021). Lower Fe/P ratios can be influenced by the depletion of iron and increased release of P into the pore water (Zak et al., 2009). In contrast, higher values signify the adsorption of P due to the formation of insoluble Fe/Mn oxides under oxic conditions (Norgbey et al., 2021), however, under the pH range of most natural waters, P has a higher affinity to Fe(III) than Mn(IV) (Bortleson and Lee, 1974). Monitoring the concentration of P in swamp deposits post-fire, particularly when events coincide with drought, is important for water quality. Increases in P concentrations can lead to eutrophication (Geurts et al., 2009; Niedermeier and Robinson, 2009). Higher Fe/P ratios for fire-affected sediments at CS-01 and UBS-01 suggest increased adsorption of P onto sediments, whilst increased release of P into the pore water is observed in fire-affected sediments at the TS-01 site. The TS-01 site shows the lowest Fe content across all samples compared to CS-01 and UBS-01, suggesting less adsorption. A number of mechanisms have been proposed for the adsorption/desorption of P, including decomposition of Fe/Mn oxides under anaerobic conditions, particle size, organic matter decomposition and changes in pH and redox potential (Bortleson and Lee, 1974; Norgbey et al., 2021), many of which have the potential to change the Fe/P ratio in these sediments.

5. Conclusion

We aimed to assess the changes in the chemistry of THPSS sediments following fire using XRD, LOI, B isotopes and major element concentration analysis. Quartz and kaolinite were the predominant minerals present due to the Hawkesbury sandstone bedrock. Calcite was also present in some of the samples. This influenced the abundance of the major element concentrations analysed, particularly Al and Mg, which were high and low, respectively, highlighting their presence in kaolinite. Small increases in the Ca/Al ratio were suggested to record the 2019–2020 bushfires; however, these increases were not preserved for older fire events, suggesting redistribution of ash-derived Ca in short succession post-fire due to the high mobility of Ca. The Mg/Al ratio also increases for fire-affected sediments, suggesting contributions from wood ash or altered mineral contributions. The P/Al and Fe/Al ratios suggested increasingly anoxic conditions with depth, likely due to greater water saturation, while fire-affected sediments at two sites (CS-01 and UBS-01) showed more oxic conditions, possibly due to altered microbial activity post-fire. Further work is needed to determine the ability of the major element concentrations of sediments to reconstruct past fire events, particularly that of older fire events and retrospective assessments of altered water quality postfire. The organic contribution to the <2 μm fraction was high across all sites, overprinting any changes in the B isotope ratio imparted to clays following a fire event. Therefore, the use of the B isotope composition of the clay-sized fraction to detect past high-severity fire events appears to be better suited to more mineral-dominated sediment deposits. In more organic-rich sediments, analysing the B isotope ratio of charcoal may be a better indicator of fire severity. Future work is needed to determine the fire severity of older recorded fire events in the Blue Mountains region to better assess ecosystem response and the potential impacts of the fire.

CRediT authorship contribution statement

Rebecca Ryan: Writing – original draft, Visualization, Methodology, Investigation, Formal analysis, Conceptualization. **Damien Lemarchand:** Writing – review & editing, Methodology, Funding acquisition. **Zoë Thomas:** Writing – review & editing, Supervision, Methodology. **Ross Bradstock:** Funding acquisition. **Anthony Dosseto:** Writing – review & editing, Supervision, Project administration, Methodology, Funding acquisition, Conceptualization.

Declaration of competing interest

The authors declare that they have no known competing financial interests or personal relationships that could have appeared to influence

the work reported in this paper.

Acknowledgements

We would like to thank NPWS for permitting site access and sample collection. Funding was provided by ARC Discovery Grant DP200101123. RR acknowledges an APA PhD scholarship and a top-up scholarship from Natural Hazards Research Australia. We would like to thank Mark Constantine, Mark Quoyle, Maame Adowa Maisie, Scott Mooney and Xiaohong Zhu for their help in the field. We also acknowledge Jose Abrantes and Lloyd White for their assistance with XRD.

Appendix A. Supplementary data

Supplementary data to this article can be found online at https://doi.org/10.1016/j.quaint.2026.110171.

Data availability

Data will be made available upon request.

References

Abney, R.B., Kuhn, T.J., Chow, A., Hockaday, W., Fogel, M.L., Berhe, A.A., 2019. Pyrogenic carbon erosion after the rim fire, Yosemite national Park: the role of burn severity and slope. J. Geophys. Res.: Biogeosciences 124, 432–449. https://doi.org/10.1029/2018JG004787.

Aryal, R., Kafley, D., Beecham, S., Morawska, L., 2018. Air quality in the Sydney metropolitan region during the 2013 Blue Mountains wildfire. Aerosol Air Qual. Res. 18, 2420–2432. https://doi.org/10.4209/aaqr.2017.10.0427.

Attiwill, P., Binkley, D., 2013. Exploring the mega-fire reality: a "Forest Ecology and Management" conference. For. Ecol. Manag. 294, 1–3. https://doi.org/10.1016/j.foreco.2012.12.025.

Belcher, C.M., New, S.L., Santín, C., Doerr, S.H., Dewhirst, R.A., Grosvenor, M.J., Hudspith, V.A., 2018. What can charcoal reflectance tell us about energy release in wildfires and the properties of pyrogenic carbon? Front. Earth Sci. 6, 1–13. https://doi.org/10.3389/feart.2018.00169.

Belmer, N., Wright, I.A., Tippler, C., 2015. Urban geochemical contamination of high conservation value upland swamps, Blue Mountains Australia. Water Air Soil Pollut. 226. https://doi.org/10.1007/s11270-015-2607-z.

Bird, M.I., Brand, M., Diefendorf, A.F., Haig, J.L., Hutley, L.B., Levchenko, V., Ridd, P.V., Rowe, C., Whinney, J., Wurster, C.M., Zwart, C., 2019. Identifying the ' savanna ' signature in lacustrine sediments in northern Australia. Quat. Sci. Rev. 203, 233–247. https://doi.org/10.1016/j.quascirev.2018.11.002.

Blevins, D.G., Lukaszewski, K.M., 1998. Boron in plant structure and function. Annu. Rev. Plant Physiol. Plant Mol. Biol. 49, 481–500. https://doi.org/10.1146/annurev.arplant.49.1.481.

Bortleson, G.C., Lee, G.F., 1974. Phosphorus, iron, and manganese distribution in sediment cores of six Wisconsin Lakes. Limnol. Oceanogr. 19, 794–801. https://doi.org/10.4319/lo.1974.19.5.0794.

Bradstock, R.A., Cohn, J.S., Gill, A.M., Bedward, M., Lucas, C., 2009. Prediction of the probability of large fires in the Sydney region of south-eastern Australia using fire weather. Int. J. Wildland Fire 18, 932–943. https://doi.org/10.1071/WF08133.

Bradstock, R.A., Hammill, K.A., Collins, L., Price, O., 2010. Effects of weather, fuel and terrain on fire severity in topographically diverse landscapes of south-eastern Australia. Landsc. Ecol. 25, 607–619. https://doi.org/10.1007/s10980-009-9443-8.

Bronk Ramsey, C., 2009. Dealing with outliers and offsets in radiocarbon dating. Radiocarbon 51, 1023–1045. https://doi.org/10.1017/s0033822200034093.

Byram, G.M., 1959. Combustion of forest fuels. In: Forest Fire: Control and Use.

Caccamo, G., Chisholm, L.A., Bradstock, R.A., Puotinen, M.L., 2012. Using remotely-sensed fuel connectivity patterns as a tool for fire danger monitoring. Geophys. Res. Lett. 39, 1–5. https://doi.org/10.1029/2011GL050125.

Canadell, J.G., Meyer, C.P., Mick Cook, G.D., Dowdy, A., Briggs, P.R., Knauer, J., Pepler, A., Haverd, V., 2021. Multi-decadal increase of forest burned area in Australia is linked to climate change. Nat. Commun. 12. https://doi.org/10.1038/s41467-021-27225-4.

Carroll, R., Reynolds, J.K., Wright, I.A., 2019. Geochemical impact of urban development on fragile freshwater wetlands. IOP Conf. Ser. Earth Environ. Sci. 344. https://doi.org/10.1088/1755-1315/344/1/012004.

Carroll, R., Reynolds, J.K., Wright, I.A., 2020. Geochemical signature of urbanisation in Blue Mountains upland swamps. Sci. Total Environ. 699, 134393. https://doi.org/10.1016/j.scitotenv.2019.134393.

Certini, G., 2005. Effects of fire on properties of forest soils: a review. Oecologia 143, 1–10. https://doi.org/10.1007/s00442-004-1788-8.

Chalson, J.M., Martin, H.A., 2009. A Holocene history of the vegetation of the Blue Mountains, New South Wales. Proc. Linn. Soc. N. S. W. 130, 77–109.

Chapple, R., Blignault, I., Fitzgerald, A., 2017. Communicating bushfire risk in the Blue Mountains: a case study of the fire stories film. Aust. J. Emerg. Manag. 32, 58–66.

Chetelat, B., Gaillardet, J., Chen, J., 2021. Dynamic of boron in forest ecosystems traced by its isotopes: a modeling approach. Chem. Geol. 560, 1–13. https://doi.org/10.1016/j.chemgeo.2020.119994.

Cividini, D., Lemarchand, D., Chabaux, F., Boutin, R., Pierret, M., 2010. From biological to lithological control of the B geochemical cycle in a forest watershed (Strengbach , Vosges). Geochem. Cosmochim. Acta 74, 3143–3163. https://doi.org/10.1016/j.gca.2010.03.002.

Collins, L., Bradstock, R.A., Penman, T.D., 2014. Can precipitation influence landscape controls on wildfire severity' A case study within temperate eucalypt forests of south-eastern Australia. Int. J. Wildland Fire 23, 9–20. https://doi.org/10.1071/WF12184.

Cook, G.D., 1994. The fate of nutrients during fires in a tropical savanna. Aust. J. Ecol. 19, 359–365. https://doi.org/10.1111/j.1442-9993.1994.tb00501.x.

Cowley, K.K.L., Fryirs, K.A.K., Cohen, T.J.T., Marx, S., Forbes, M., Krogh, M., Cowley, K. K.L., Cohen, K.A., Marx, T.J., Forbes, S., Krogh, M., 2020. Upland peatlands of Eastern Australia as important water storage reservoirs. Proc. Linn. Soc. N. S. W. 142, 67–76.

Cowley, K.L., Fryirs, K.A., 2020. Forgotten peatlands of eastern Australia: an unaccounted carbon capture and storage system. Sci. Total Environ. 730, 139067. https://doi.org/10.1016/j.scitotenv.2020.139067.

Cowley, K.L., Fryirs, K.A., Hose, G.C., 2018. The hydrological function of upland swamps in eastern Australia: the role of geomorphic condition in regulating water storage and discharge. Geomorphology 310, 29–44. https://doi.org/10.1016/j.geomorph.2018.03.004.

Cunningham, C.J., 1984. Recurring natural fire hazards : a case study of the Blue Mountains, New South Wales, Australia. Appl. Geogr. 4, 5–27. https://doi.org/10.1016/0143-6228(84)90002-X.

D'Costa, D.M., Kershaw, A.P., 1995. A late Pleistocene and Holocene pollen record from Lake Terang, Western plains of Victoria, Australia. Palaeogeogr. Palaeoclimatol. Palaeoecol. 113, 57–67. https://doi.org/10.1016/0031-0182(95)00062-Q.

Daniell, T., White, I., 2005. Bushfires and their implications for management of future water supplies in the Australian Capital Territory. Climatic and Anthropogenic Impacts on the Variability of Water Resources, pp. 22–24.

Demeyer, A., Voundi Nkana, J.C., Verloo, M.G., 2001. Characteristics of wood ash and influence on soil properties and nutrient uptake: an overview. Bioresour. Technol. 77, 287–295. https://doi.org/10.1016/S0960-8524(00)00043-2.

Dikici, H., Yilmaz, C.H., 2006. Peat fire effects on some properties of an artificially drained peatland. J. Environ. Qual. 35, 866–870. https://doi.org/10.2134/jeq2005.0170.

Etiegni, L., Campbell, A.G., 1991. Physical and chemical characteristics of wood ash. Bioresour. Technol. 37, 173–178.

Fleet, M.E.L., 1965. Preliminary investigations into the sorption of boron by clay minerals. Clay Miner. 6, 3–16. https://doi.org/10.1180/claymin.1965.006.1.02.

Flinn, D.W., Hopmans, P., Farrell, P.W., James, J.M., 1979. Nutrient loss from the burning of Pinus radiata logging residue. Aust. For. Res. 9, 17–23.

Francos, M., Úbeda, X., Pereira, P., 2020. Long-term forest management after wildfire (Catalonia, NE Iberian Peninsula). J. For. Res. 31, 269–278. https://doi.org/10.1007/s11676-018-0867-3.

Freidman, B.L., Fryirs, K.A., 2015. Rehabilitating upland swamps using environmental histories: a case study of the Blue Mountains peat swamps, Eastern Australia. Geografiska Annaler, Series A. Phys. Geogr. 97, 337–353. https://doi.org/10.1111/geoa.12068.

Fryirs, K., Freidman, B., Williams, R., Jacobsen, G., 2014a. Peatlands in eastern Australia? Sedimentology and age structure of temperate highland peat swamps on sandstone (THPSS) in the Southern highlands and Blue Mountains of NSW, Australia. Holocene 24, 1527–1538. https://doi.org/10.1177/0959683614544064.

Fryirs, K., Gough, J., Hose, G.C., 2014b. The geomorphic character and hydrological function of an upland swamp, Budderoo Plateau, southern highlands, NSW, Australia. Phys. Geogr. 35, 313–334. https://doi.org/10.1080/02723646.2014.890092.

Fryirs, K.A., Cowley, K.L., Hejl, N., Chariton, A., Christiansen, N., Dudaniec, R.Y., Farebrother, W., Hardwick, L., Ralph, T., Stow, A., Hose, G., 2021. Extent and effect of the 2019-20 Australian bushfires on upland peat swamps in the Blue Mountains, NSW. Int. J. Wildland Fire 30, 294–300. https://doi.org/10.1071/WF20081.

Gaillardet, J., Lemarchand, D., 2009. Boron in the weathering environment. In: Boron Isotopes, pp. 1–26.

Gaillardet, J., Lemarchand, D., Göpel, C., Manhès, G., 2001. Evaporation and sublimation of boric acid: application for boron purification from organic rich solutions. Geostand. Newsl. 25, 67–75. https://doi.org/10.1111/j.1751-908X.2001.tb00788.x.

Gangjian, W., Jingxian, W., Ying, L., Ting, K., Zhongyuan, R., Jinlonga, M., Yigang, X., 2013. Measurement on high-precision boron isotope of silicate materials by a single column purification. J. Anal. At. Spectrom. 28, 606–612. https://doi.org/10.1039/c3ja30333k.

Geilert, S., Vogl, J., Rosner, M., Voerkelius, S., Eichert, T., 2015. Mass spectrometry & purification techniques boron isotope fractionation in bell pepper. Mass Spectromet. Purificat. Tech. 1, 1–6. https://doi.org/10.4172/mso.1000101.

Geurts, J.J.M., Sarneel, J.M., Willers, B.J.C., Roelofs, J.G.M., Verhoeven, J.T.A., Lamers, L.P.M., 2009. Interacting effects of sulphate pollution, sulphide toxicity and eutrophication on vegetation development in fens: a mesocosm experiment. Environ. Pollut. 157, 2072–2081. https://doi.org/10.1016/j.envpol.2009.02.024.

Gibson, R., Danaher, T., Hehir, W., Collins, L., 2020. A remote sensing approach to mapping fire severity in south-eastern Australia using sentinel 2 and random forest. Rem. Sens. Environ. 240, 111702. https://doi.org/10.1016/j.rse.2020.111702.

Goldberg, S., Suarez, D.L., 2012. Role of organic matter on boron adsorption-desorption hysteresis of soils. Soil Sci. 177, 417–423. https://doi.org/10.1097/SS.0b013e318256bc0c.

Goli, E., Hiemstra, T., Rahnemaie, R., 2019. Interaction of boron with humic acid and natural organic matter: experiments and modeling. Chem. Geol. 515, 1–8. https://doi.org/10.1016/j.chemgeo.2019.03.021.

Goodarzi, F., Swaine, D.J., 1994. The influence of geological factors on the concentration of boron in Australian and Canadian coals. Chem. Geol. 118, 301–318. https://doi.org/10.1016/0009-2541(94)90183-X.

Guénon, R., Vennetier, M., Dupuy, N., Roussos, S., Pailler, A., Gros, R., 2013. Trends in recovery of mediterranean soil chemical properties and microbial activities after infrequent and frequent wildfires. Land Degrad. Dev. 24, 115–128. https://doi.org/10.1002/ldr.1109.

Hammill, K., Tasker, L., Barker, C., 2013. The invisible mosaic : fire regimes in one of NSW's Most iconic conservation areas. In: Proceedings from the 9th Biennial NCCNSW Bushfire Conference, p. 13.

Hammill, K.A., Bradstock, R.A., 2006. Remote sensing of fire severity in the Blue Mountains: influence of vegetation type and inferring fire intensity. Int. J. Wildland Fire 15, 213–226. https://doi.org/10.1071/WF05051.

Hardwick, L.J., 2020. Functional Ecological Processes in Upland Swamps and Chain of Ponds Systems in the Blue Mountains and Southern Highlands of Eastern New South Wales, Australia. Macquarie Univeristy. https://doi.org/10.25949/19444391.v1.

Hemming, N.G., Hanson, G.N., 1992. Boron Isotopic Composition and Concentration in Modern Marine Carbonates, vol. 56, pp. 537–543.

Hinrichs, J., Schnetger, B., Schale, H., Brumsack, H.J., 2001. A high resolution study of NE Atlantic sediments at station Bengal: geochemistry and early diagenesis of Heinrich layers. Mar. Geol. 177, 79–92. https://doi.org/10.1016/S0025-3227(01)00125-6.

Keeley, J.E., 2009. Fire intensity, fire severity and burn severity: a brief review and suggested usage. Int. J. Wildland Fire 18, 116–126. https://doi.org/10.1071/WF07049.

Keeley, J.E., Syphard, A.D., 2016. Climate change and future fire regimes: examples from California. Geosciences (Switzerland) 6, 1–14. https://doi.org/10.3390/geosciences6030037.

Keith, D.A., Myerscough, P.J., 1993. Floristics and soil relations of upland swamp vegetation near Sydney. Aust. J. Ecol. 18, 325–344. https://doi.org/10.1111/j.1442-9993.1993.tb00460.x.

Keith, D.A., Benson, D.H., Baird, I.R.C., Watts, L., Simpson, C.C., Krogh, M., Gorissen, S., Ferrer-Paris, J.R., Mason, T.J., 2023. Effects of interactions between anthropogenic stressors and recurring perturbations on ecosystem resilience and collapse. Conserv. Biol. 37, 1–14. https://doi.org/10.1111/cobi.13995.

Khanna, P.K., Raison, R.J., Falkiner, R., 1994. Chemical properties of ash derived from Eucalyptus litter and its effects on forest soils. For. Ecol. Manag. 66, 107–125. https://doi.org/10.1016/0378-1127(94)90151-1.

Kjaergaard, C., Heiberg, L., Jensen, H.S., Hansen, H.C.B., 2012. Phosphorus mobilization in rewetted peat and sand at variable flow rate and redox regimes. Geoderma 173–174, 311–321. https://doi.org/10.1016/j.geoderma.2011.12.029.

Könönen, M., Jauhiainen, J., Laiho, R., Kusin, K., Vasander, H., 2015. Physical and chemical properties of tropical peat under stabilised land uses. Mires Peat 16.

Lampela, M., Jauhiainen, J., Vasander, H., 2014. Surface peat structure and chemistry in a tropical peat swamp forest. Plant Soil 382, 329–347. https://doi.org/10.1007/s11104-014-2187-5.

Lemarchand, D., Cividini, D., Turpault, M., Chabaux, F., 2012. Boron isotopes in different grain size fractions : exploring past and present water – rock interactions from two soil profiles (Strengbach, Vosges Mountains). Geochem. Cosmochim. Acta 98, 78–93. https://doi.org/10.1016/j.gca.2012.09.009.

Liaghati, T., Preda, M., Cox, M., 2003. Heavy metal distribution and controlling factors within coastal plain sediments. Bells Creek catchment , southeast Queensland , Australia 29, 935–948. https://doi.org/10.1016/S0160-4120(03)00060-6.

Lu, S., Dosseto, A., Lemarchand, D., Dlapa, P., Simkovic, I., Bradstock, R., 2022. Investigating boron isotopes and FTIR as proxies for bushfire severity. Catena, 106621. https://doi.org/10.1016/j.catena.2022.106621, 1–15.

Lu, S., Dosseto, A., Lemarchand, D., 2024. Boron in wildfires : new insights into boron isotope fractionation during volatilisation, leaching and adsorption after combustion. Geochem. Cosmochim. Acta 379, 208–218.

Malone, S.L., Kobziar, L.N., Staudhammer, C.L., Abd-Elrahman, A., 2011. Modeling relationships among 217 fires using remote sensing of burn severity in southern pine forests. Remote Sens. 3, 2005–2028. https://doi.org/10.3390/rs3092005.

Mayland, H.F., Wilkinson, S.R., 1989. Soil factors affecting magnesium availability in plant-animal systems: a review. J. Anim. Sci. 67, 3437–3444.

McLauchlan, K.K., Higuera, P.E., Miesel, J., Rogers, B.M., Schweitzer, J., Shuman, J.K., Tepley, A.J., Varner, J.M., Veblen, T.T., Adalsteinsson, S.A., Balch, J.K., Baker, P., Batllori, E., Bigio, E., Brando, P., Cattau, M., Chipman, M.L., Coen, J., Crandall, R., Daniels, L., Enright, N., Gross, W.S., Harvey, B.J., Hatten, J.A., Hermann, S., Hewitt, R.E., Kobziar, L.N., Landesmann, J.B., Loranty, M.M., Maezumi, S.Y., Mearns, L., Moritz, M., Myers, J.A., Pausas, J.G., Pellegrini, A.F.A., Platt, W.J., Roozeboom, J., Safford, H., Santos, F., Scheller, R.M., Sherriff, R.L., Smith, K.G., Smith, M.D., Watts, A.C., 2020. Fire as a fundamental ecological process: research advances and frontiers. J. Ecol. 108, 2047–2069. https://doi.org/10.1111/1365-2745.13403.

McParland, L.C., Collinson, M.E., Scott, A.C., Campbell, G., 2009. The use of reflectance values for the interpretation of natural and anthropogenic charcoal assemblages. Archaeol. Anthropol. Sci. 1, 249–261. https://doi.org/10.1007/s12520-009-0018-z.

Mouillot, F., Field, C.B., 2005. Fire history and the global carbon budget: a 1° × 1° fire history reconstruction for the 20th century. Glob. Change Biol. 11, 398–420. https://doi.org/10.1111/j.1365-2486.2005.00920.x.

Natalicchio, M., Pierre, F. Dela, Birgel, D., Brumsack, H., Carnevale, G., Gennari, R., Gier, S., Lozar, F., Pellegrino, L., Sabino, M., Schnetger, B., Peckmann, J., 2019. Paleoenvironmental change in a precession-paced succession across the onset of the Messinian salinity crisis: insight from element geochemistry and molecular fossils. Palaeogeogr. Palaeoclimatol. Palaeoecol. 518, 45–61. https://doi.org/10.1016/j.palaeo.2019.01.009.

Nedkov, R., Molla, I., Velizarova, E., Radeva, K., 2018. Application of remote sensing data for forest fires severity assessment. Earth Resources and Environmental Remote Sensing/GIS Application IX 65, 10790. https://doi.org/10.1117/12.2325742.

Niedermeier, A., Robinson, J.S., 2009. Phosphorus dynamics in the ditch system of a restored peat wetland. Agric. Ecosyst. Environ. 131, 161–169. https://doi.org/10.1016/j.agee.2009.01.011.

Nolan, R.H., Boer, M.M., Resco De Dios, V., Caccamo, G., Bradstock, R.A., 2016. Large-scale, dynamic transformations in fuel moisture drive wildfire activity across southeastern Australia. Geophys. Res. Lett. 43, 4229–4238. https://doi.org/10.1002/2016GL068614.

Norgbey, E., Li, Y., Zhu, Y., Nwankwegu, A.S., Bofah-Buah, R., Nuamah, L., 2021. Seasonal dynamics of iron and phosphorus in reservoir sediments in Eucalyptus plantation region. Ecol. Process. 10. https://doi.org/10.1186/s13717-021-00280-x.

Park, H., Schlesinger, W.H., 2002. Global biogeochemical cycle of boron. Glob. Biogeochem. Cycles 16. https://doi.org/10.1029/2001gb001766, 20-1–20-11.

Pereira, P., Úbeda, X., Martin, D.A., 2012. Fire severity effects on ash chemical composition and water-extractable elements. Geoderma 191, 105–114. https://doi.org/10.1016/j.geoderma.2012.02.005.

Quintana, J.R., Cala, V., Moreno, A.M., Parra, J.G., 2007. Effect of heating on mineral components of the soil organic horizon from a Spanish juniper (Juniperus thurifera L.) woodland. J. Arid Environ. 71, 45–56. https://doi.org/10.1016/j.jaridenv.2007.03.002.

Rönspieß, L., Dellwig, O., Lange, X., Nausch, G., Schulz-Bull, D., 2020. Spatial and seasonal phosphorus dynamics in a eutrophic estuary of the southern Baltic Sea. Estuar. Coast Shelf Sci. 233. https://doi.org/10.1016/j.ecss.2019.106532.

Roux, P., Lemarchand, D., Hughes, H.J., Turpault, M., 2015. A rapid method for determining boron concentration (ID-ICP-MS) and δ11B (MC-ICP-MS) in vegetation samples after microwave digestion and cation exchange chemical purification. Geostand. Geoanal. Res. 39, 453–466. https://doi.org/10.1111/j.1751-908X.2014.00328.x.

Roux, P., Lemarchand, D., Redon, P.-O., Turpault, M.-P., 2022. B and δ11B biogeochemical cycle in a beech forest developed on a calcareous soil: pools, fluxes, and forcing parameters. Sci. Total Environ. 806, 150396. https://doi.org/10.1016/j.scitotenv.2021.150396.

Ryan, R., Dosseto, A., Lemarchand, D., Dlapa, P., Thomas, Z., Simkovic, I., Bradstock, R., 2023. Boron isotopes and FTIR spectroscopy to identify past high severity fires. Catena 222. https://doi.org/10.1016/j.catena.2022.106887.

Ryan, R., Thomas, Z., Simkovic, I., Dlapa, P., Worthy, M., Wasson, R., Bradstock, R., Mooney, S., Haynes, K., Dosseto, A., 2024. Assessing changes in high-intensity fire events in south-eastern Australia using Fourier Transform Infra-red (FITR) spectroscopy. Int. J. Wildland Fire 33, 1–15. https://doi.org/10.1071/WF24064.

Ryan, R., Dosseto, A., Dlapa, P., Thomas, Z., Simkovic, I., Mooney, S., Bradstock, R., 2025. Using Fourier Transform Infrared spectroscopy to produce high-resolution centennial records of past high-intensity fires from organic-rich sediment deposits. Int. J. Wildland Fire 34. https://doi.org/10.1071/WF23175.

Sawyer, R., Bradstock, R., Bedward, M., Morrison, R.J., 2018. Soil carbon in Australian fire-prone forests determined by climate more than fire regimes. Sci. Total Environ. 639, 526–537. https://doi.org/10.1016/j.scitotenv.2018.05.169.

Sharples, J.J., Cary, G.J., Fox-Hughes, P., Mooney, S., Evans, J.P., Fletcher, M.S., Fromm, M., Grierson, P.F., McRae, R., Baker, P., 2016. Natural hazards in Australia: extreme bushfire. Clim. Change 139, 85–99. https://doi.org/10.1007/s10584-016-1811-1.

Smith, B.H., Emerson, W.W., 1976. Exchangeable aluminium on kaolinite. Aust. J. Soil Res. 14, 43–53.

Sulwiński, M., Mętrak, M., Wilk, M., Suska-Malawska, M., 2020. Smouldering fire in a nutrient-limited wetland ecosystem: long-Lasting changes in water and soil chemistry facilitate shrub expansion into a drained burned fen. Sci. Total Environ. 746. https://doi.org/10.1016/j.scitotenv.2020.141142.

Sundararajan, M., Natesan, U., 2010. Geochemistry of core sediments from Mullipallam creek, south east coast of India. Environ. Earth Sci. 61, 947–961. https://doi.org/10.1007/s12665-009-0414-9.

Sundararajan, M., Srinivasalu, S., 2010. Geochemistry of core sediments from Gulf of Mannar, India. Int. J. Environ. Res. 4, 861–876.

Vengosh, A., Chivas, A.R., McCulloch, M.T., Starinsky, A., Kolodny, Y., 1991. Boron isotope geochemistry of Australian salt lakes. Geochem. Cosmochim. Acta 55, 2591–2606.

Vogl, J., Rosner, M., 2012. Production and certification of a unique set of isotope and Delta reference materials for boron isotope determination in geochemical, environmental and industrial materials. Geostand. Geoanal. Res. 36, 161–175. https://doi.org/10.1111/j.1751-908X.2011.00136.x.

Weiss, D., Shotyk, W., Rieley, J., Page, S., Gloor, M., Reese, S., Martinez-Cortizas, A., 2002. The geochemistry of major and selected trace elements in a forested peat bog, Kalimantan, SE Asia, and its implications for past atmospheric dust deposition. Geochem. Cosmochim. Acta 66, 2307–2323. https://doi.org/10.1016/S0016-7037(02)00834-7.

Wilkinson, M.T., Chappell, J., Humphreys, G.S., Fifield, K., Smith, B., Hesse, P., 2005. Soil production in heath and forest, Blue Mountains, Australia: influence of lithology and palaeoclimate. Earth Surf. Process. Landf. 30, 923–934. https://doi.org/10.1002/esp.1254.

Williams, L.B., Hervig, R.L., Holloway, J.R., Hutcheon, I., 2001. Boron isotope geochemistry during diagenesis . Part I . Experimental determination of fractionation during illitization of smectite. Geochem. Cosmochim. Acta 65, 1769–1782.

Xiao, J., Vogl, J., Rosner, M., Jin, Z., 2022. Boron isotope fractionation in soil-plant systems and its influence on biogeochemical cycling. Chem. Geol. 606, 120972. https://doi.org/10.1016/j.chemgeo.2022.120972.

Xu, Q., Dong, Y., Zhu, H., Sun, A., 2015. Separation and Analysis of Boron Isotope in High Plant by Thermal Ionization Mass Spectrometry, vol 2015. Hindawi Publishing Corporation, pp. 1–6.

Yermiyahu, U., Keren, R., Chen, Y., 2001. Effect of composted organic matter on boron uptake by plants. Soil Sci. Soc. Am. J. 65, 1436–1441. https://doi.org/10.2136/sssaj2001.6551436x.

Zak, D., Rossoll, T., Exner, H.J., Wagner, C., Gelbrecht, J., 2009. Mitigation of sulfate pollution by rewetting of fens - a conflict with restoring their phosphorus sink function? Wetlands 29, 1093–1103. https://doi.org/10.1672/09-102D.1.

Zhang, Y., Lim, S., Sharples, J.J., 2017. Wildfire occurrence patterns in ecoregions of New South Wales and Australian Capital Territory, Australia. Nat. Hazards 87, 415–435. https://doi.org/10.1007/s11069-017-2770-1.